Modelling of Asymmetric Incommensurable Torque Signals

L. Kurmann[1,2], P. Grubert[2]
[1]University of Freiburg, IMTEK, Germany
[2]University of Applied Sciences and Arts Northwestern Switzerland (FHNW), Switzerland

Abstract

Asymmetric incommensurable torque (AIT) signals, are signals, that are asymmetric as well as unbalanced, e.g. incommensurable over one revolution. They can be achieved by exploiting magnetic nonpolar repulsion techniques [1], [2], [3], aiming at designing kinetic energy harvester (KEH) systems. In this paper we focus on the modelling of such AIT signals without focusing on the dynamics used in KEH systems, see also [1], [3]. AIT signals can be approximated with several methods and all shown calculations are in full agreement with the classical Electromagnetic Theory. The first method is based on time consuming full 3D FE generated torque and force signals. The second method is using also FE generated torque and force signals, but they are calculated only in orthogonal directions, approximated with Fourier Series and normalized to provide 2D stiffness signals. The third approach focuses on filamentary current rings to calculate the magnetic field of permanent magnets (PMs) to generate in a purely analytical way the same force and torque signals as in the previous methods.

Introduction

Energy Harvesting is a technology for capturing non-electrical energy from ambient energy sources, converting it into electrical energy and storing it to power wireless electronic devices [4–10]. The process of capturing mechanical energy such as shocks and vibrations is a subject area of energy harvesting requiring specific types of devices, so called kinetic energy harvesters (KEH) and there are many types of KEHs, [10–16]. AIT signals aimed to be used in KEH systems, employing here still the naming convention KEH, as effectively rotor mass and rotor inertia are used to start an everlasting oscillation in theory. While searching for energy harvesting opportunities and motivated by the ideas in [17], we focused on modelling nonlinear PM spring systems with rotary and translatory DoFs.

To achieve AIT-, or unbalanced torque-signals, several systems can be envisaged, the simplest is shown in Figure 1, consisting of one rotor PM and one stator PM. The rotor PM is revolving with ϕ and accompanied with at least one additional DoF, either radially in r direction or axially in z direction (or in r as well as z direction).

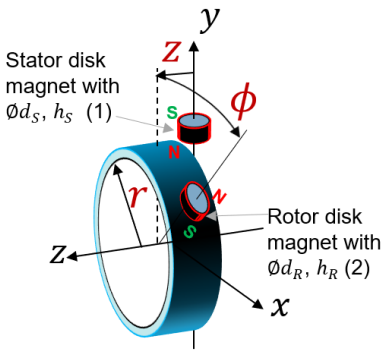

Figure 1. 1-3DoF rotary-translatory shaft movement with one stator-rotor disk PM magnet pair

It is important to use a well-deliberate closed rotor PM trajectory to create an AIT signal. To do so, we need to define first the stiffness signal in all spatial directions.

Problem Definition and Governing Equations

First, it is most important to define the following assumptions for this modelling exercise.

$$\mathbf{F_{mag}} = q\big(\mathbf{E} + (\mathbf{v} \times \mathbf{B})\big) \cong q(\mathbf{v} \times \mathbf{B}) \qquad (1)$$

The resulting magnetic force $\mathbf{F_{mag}}$ from the Lorentz force law is calculated given the charge q, the electric field- **E**, the magnetic field- **B** and the velocity-vector **v**. As in these KEH systems, velocities are extremely slow in respect to the speed of light, **E** can be set zero (which is always assumed in calculations for electrical machines, see for instance [18]). Generally, magnetic forces will do no work on isolated electric charges [19], as a point charge has no dimensional extension and therefore, the created velocity **v** due to the PM rendez-vous is in the same direction as the trajectory velocity $\mathbf{v_0}$ of the rotor.

$$W_{mag} = \int \mathbf{F_{mag}} \cdot d\mathbf{l} \xrightarrow{d\mathbf{l}=\mathbf{v_0}dt} \int \boldsymbol{q}(\mathbf{v} \times \mathbf{B}) \cdot \mathbf{v_0} dt = 0 \qquad (2)$$

For the PM-based KEH systems proposed in this paper, we show that the calculated magnetic work W_{mag} is unequal zero by applying three different methods and using (a) well-deliberated closed trajectories Γ, and (b) instead of using a point charge, a disk PM or a current loop (both having geometrical extensions). So, in contrast to (2),

$$W_{mag} = \int \mathbf{F_{mag}} \cdot d\mathbf{l} \neq 0 \qquad (3)$$

The creation of stiffness signals for the nonlinear PM spring shown in Figure 1, we create first orthogonally placed FE torque and force signals, shown in Figure 2. They represent torque and force signals from disk magnets (the same disk PM geometry used on stator and rotor; air gap of PM pair is kept $1mm$ for all simulations, if not otherwise mentioned; N52 disk magnets, residual magn. $B \cong 1.445T$, $d_R = d_S = 10mm$ and $h_R = h_S = 5mm$; radius $r_0 = 27mm$ from origin to the center of mass of each PM). In case we have two, three or four symmetrically placed PMs on the circumference of the rotor and stator, the created torque and force signal is two- three- or fourfold. By means of using the Maxwell Stress Tensor σ, the normal vector pointing out from the PM $\boldsymbol{n}$ and calculating the resulting force **F** resp. torque $\boldsymbol{\tau}$ over the corresponding surfaces S.

$$\boldsymbol{F} = \oint_S \boldsymbol{n}\, \sigma\, dS \tag{4}$$

$$\boldsymbol{\tau} = \boldsymbol{r} \times \boldsymbol{F} \tag{5}$$

Note, that (4) is an identity to the otherwise necessary volume integral. This calculation is valid, as we deal in such KEH applications in quasi static field environments – if we keep the rotor revolution slow enough and no additional energy by E-fields is considered (1). (Whether the rotor is rotating with one revolution per year or one revolution per ms, it is well below the propagation velocity of speed of light and accompanied **E**-fields can be neglected. In case the rotor is revolving much faster, in the order of $< 1\mu s$, such **E** -fields must be considered and the KEH system becomes an antenna.) Such static fields can be computed with FE methods, setting

$$\nabla \cdot \mathbf{B} = 0 \tag{6}$$

The problem definition is given with (4)-(6) in the COMSOL GUI environment, using the magnetic fields, no current interface (mfnc).

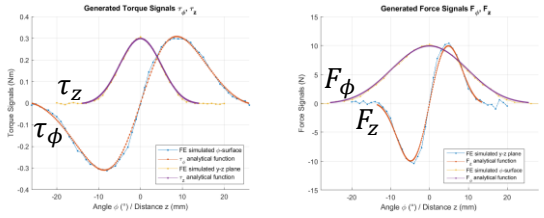

(a) (b)

Figure 2. FE COMSOL simulated rotary shaft torque (a) and shaft force in z direction (b) using one stator-rotor PM pair, situation shown in Figure 1.

The shown orthogonal static (mfnc) FE simulated four torque/force signals in ϕ and z direction are shown in Figure 2. The physical meaning is explained exemplarily with the signal τ_ϕ: there needs to be mechanical torque energy pumped into the rotor, reaching the maximum negative torque of $\tau_{max-} \cong -0.305Nm$ at $\phi \cong -8°$ and reaching at $\phi = 0°$ the instable point where for $\phi > 0°$ rotor starts accelerating until reaching $\tau_{max+} \cong +0.305Nm$ (with maximal velocity close to $\phi = 26°$). The torque envelope signal (τ_z) is created by using first an FE computed torque signal (orange curve; keeping the torque angle at its maximum $|\phi| \cong 8°$ and sweeping subsequently with this fixed torque angle) in the axial z direction; the force signals F_ϕ and F_z are created alike. Also depicted in Figure 2 are the Fourier-Series approximated signals, with even functions for τ_z, F_ϕ and odd functions for τ_ϕ, F_z. The 4th order normalized torque and force signals are

$$\begin{aligned} f_\tau(\phi, z) &\cong f_{\tau rad}(\phi)\, f_{\tau ax}(z) \\ &= \left(\sum_{n_\tau=1}^{4} b_{n_\tau} \sin\left(n_\tau\, \omega_{\phi_\tau}\, \phi\right)\right)\left(a_{0_\tau} \right. \\ &\left. + \sum_{n_\tau=1}^{4} a_{n_\tau} \cos\left(n_\tau\, \omega_{z_\tau}\, z\right)\right) \end{aligned} \tag{7}$$

$$\begin{aligned} f_F(\phi, z) &\cong f_{Fax}(z) f_{Frad}(\phi) \\ &= \left(\sum_{n_f=1}^{4} b_{n_f} \sin\left(n_f\, \omega_{\phi_f}\, z\right)\right)\left(a_{0_f} \right. \\ &\left. + \sum_{n_f=1}^{4} a_{n_f} \cos\left(n_f\, \omega_{z_f}\, \phi\right)\right) \end{aligned} \tag{8}$$

The corresponding 2D torque and force signals can also be written as

$$\tau_{rad}(\phi, z) = C_r\, f_\tau(\phi, z) \tag{9}$$

$$F_{ax}(\phi, z) = k_r\, f_F(\phi, z) \tag{10}$$

with introduced stiffness constants C_r (Nm/rad) and k_r (N/m). They can be easily measured as the maximum break-torque respectively break-force. Figure 3 show these normalized 2D amplitude diagrams for the stiffnesses f_τ, f_F for the torque- and force-signals.

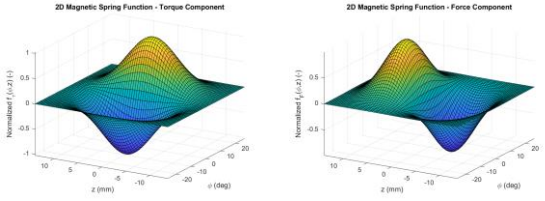

(a) (b)

Figure 3. Normalized 2D torque spring- (a) and force spring- (b) amplitude for ϕ and z direction, eq. (9) and (10)

Note that outside the shown intervals of Figure 3, the torque-, force-signals are approximated to be zero. By introducing an axial cam movement

$$z_R(\phi) = A_{co} \sin(\omega_{co}\, \phi + \xi_{co}) \tag{11}$$

where the lateral movement z_R is constrained to the rotating DoF ϕ with a given cam amplitude A_{co}, an initial offset ξ_{co} and an angular velocity ω_{co}. In Figure 4 a stator-rotor configuration with two rotor magnets (green dots) and three stator magnets (blue dots) are

considered. The axial movement is locked in a harmonic cam movement (green lines) following (11),

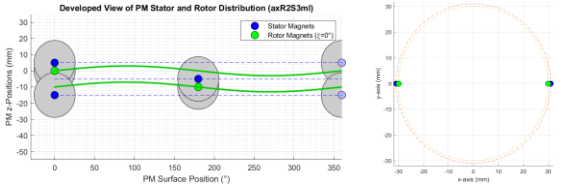

(a) (b)

Figure 4. Stator-rotor PM configuration axR2S3ml in developed view keeping the stator and rotor PM distances to each other at $10mm$ (a) and front view (b) with axial z-direction harmonic wobbling rotor.

applying $A_{co} = 3mm$, $\xi_{co} = 0$ and $\omega_{co} = 1$. The imposed cam-based trajectory velocity vector $\mathbf{v_0}$, follows

$$\mathbf{v_0} = \frac{\mathrm{d}}{\mathrm{d}t}\begin{pmatrix} r_0 \cos\phi(t) \\ r_0 \sin\phi(t) \\ z_R(\phi(t)) \end{pmatrix} \tag{12}$$

In contrast to (2), this cam-based trajectory velocity $\mathbf{v_0}$ is not equal to the resulting 'natural' trajectory velocity vector $\mathbf{v}$ when no cam is applied (during a stator-rotor PM rendez-vous with a PM that has geometrical extension). The dynamic motion of such a configured rotor system can be derived using Lagrange approach, see also [1, 3].

Numerical Models and Results

The torque response on a stiff rotor with one stator-rotor PM pair shown in Figure 2a can also be modeled with two axis symmetrical stator-rotor PM pairs in the same plane, shown in Figure 5a. In Figure 5b, again a stiff rotor with two rotor PMs is shown, this time the rotor PMs are not located in the same plane – simulation setup for model shown in Figure 4 (and a full 3D simulation is necessary, as the rotor PMs wobble in the z-axis with eq. (11)).

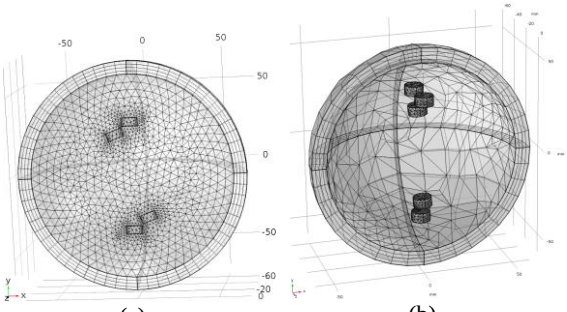

(a) (b)

Figure 5. Meshed geometry setups in FE COMSOL PM 3D simulations (mm). The inner PMs sit on an invisible (stiff) rotor. In (a) a z-axis symmetric mesh is shown; (b) depicts a full 3D mesh simulation setup.

Both models were simulated with magnetic fields no currents (mfnc) for stationary torque and force response. It has been verified that such static simulations are sufficient accurate for validating torque responses in PM setups [20]. Depending on the stator-rotor PM setup, it might be necessary to simulate statically the torque response from 0°…359° in 1° steps to accurately calculate the resulting torque signal. This is computationally intensive, using the Maxwell surface stress tensor method in COMSOL. The remedy to safe computing time is the introduced Fourier-Series method, see also [1]. Furthermore, it allows to do parameter sweeps, approximately 6000-times faster than FE COMSOL calculations.

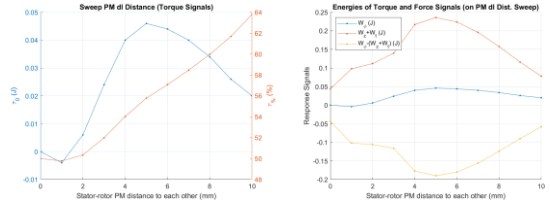

(a) (b)

Figure 6. Resulting torque signals eq. (13) and accumulated energies eq. (14)-(16) by sweeping dl for stator-rotor PM configuration axR2S3ml and using a cam radius of $r_{cam} = 15mm$.

Figure 6 depicts such an example sweep, where the z-distance for the stator PMs to each other (the dl-distance, see also Figure 4a) is successively increased from $0,2,4 \ldots,20mm$ and simultaneously the wobbling rotor PMs are kept symmetrical in between the dashed blue stator PM lines. This method has also the great advantage that any PM geometry can be approximated – if in advance with an FE tool the accordingly orthogonal Fourier-Series parameters have been identified.

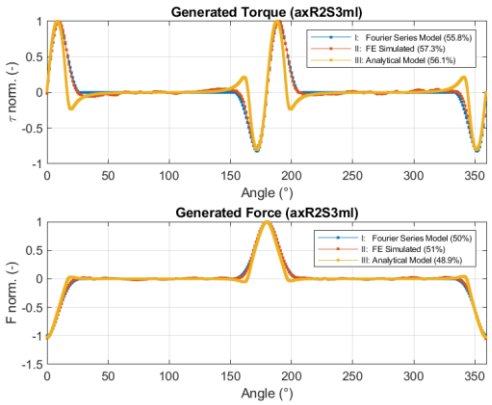

Figure 7. Resulting normalized torque and force signals from setup in Figure 4 (Figure 5b).

However, in case the PM geometry is limited to shapes of disk magnets (with magnetization direction parallel to the cylinder height), there are also purely analytical methods available, such as Biot-Savart law approach [21] or the Lorentz approach [22] – both methods are common to emulate purely analytically the magnet fields of permanent magnets [23]. The analytical force calculations for two filamentary (2D) current loops in any desired inclined 3D space position to each other are demanding to calculate (such forces could also be

calculated in 3D coil structures, approximating better the static magnetic field **B** of a PM, but the analytical calculations are becoming most demanding to do and the force accuracy improvements are small.) Figure 7 compares three different normalized torque and force calculations. The 1st (I) method using the Fourier-Series approach, the 2nd (II), using the standard COMSOL method and the 3rd (III), described in [22]. However, only the 2nd method is calculating also the expected torque and force signals, which can be used for validation purposes (in the configuration axR2S3ml, the peak torque, force signals close to $0.31Nm$, resp. $20N$). The % in the legend indicates the asymmetry of the according signal, where 50% indicates a balanced torque/force signal. The torque signal is clearly asymmetric and incommensurable (over one revolution). Figure 8a depicts customized PM geometry in the stator-rotor configuration shown in Figure 4 and Figure 5b. The two identical rotor magnets have a length (x) of $20mm$, a depth (z) of $4mm$ and a max. height (y) of $12mm$ (radius from origin to the rotor magnet tip $29.5mm$), optimized airgap of $0.5mm$ (instead of $1mm$). The three identical stator magnets have the same dimensions as the rotor magnets, except for the height ($13mm$ in the center to the top); magnetization in the same as the disk magnets. Figure 8b shows the resulting COMSOL computed torque signals, disk PM vs. customized PM geometry. Using a customized PM geometry can enhance the asymmetric incommensurable torque signal considerably.

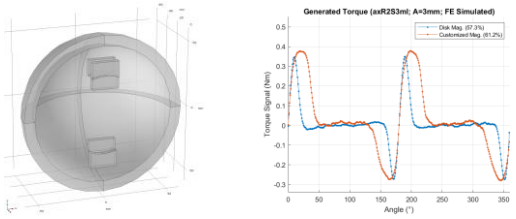

(a) (b)

Figure 8. Geometry setup (a) in FE COMSOL PM 3D simulations (mm); comparison of resulting torque signals (b) between disk PM and customized PM geometry.

The forecasted torque energy surplus W_ϕ, in stator-rotor configuration axR2S3ml is $46.1mJ$, using

$$W_\phi = \int_0^{2\pi} (1 - \mu_{rad})\tau(\phi)\, d\phi \qquad (13)$$

with the radial damping coefficient $\mu_{rad} = 0$ (no damping) and $\tau(\phi)$, the AIT signal. The accompanied lateral z-force component ($|F(\phi)| \cong F_N$, if the amplitude is kept small enough) over one revolution is approximately zero and therefore also its energy component, given

$$W_z \cong \int_0^{2\pi} \mu_{ax} |F(\phi)|\, z_R(\phi)\, d\phi \cong 0 \qquad (14)$$

with μ_{ax} the axial damping coefficient and $z_R(\phi)$ given in (11). It has been shown in [3], that this approximation is nearly exact also dynamically (over one revolution), even when considering nonlinear friction models, e.g. $\mu_{ax} \to \mu_{ax}(\phi')$, see [24]. The corresponding tangential energy component W_t becomes $234.6mJ$, using

$$W_t \cong \int_0^{2\pi} \mu_{ax} |F(\phi)|\, r_{cam}\, d\phi \qquad (15)$$

This energy component needs to be accordingly damped to generate an energy surplus. Note, that for (13)-(15) the mfnc FE COMSOL approximated signals τ, F of Figure 7 have been used to calculate the energies. If the damping coefficient $\mu_{ax} = 1$ (maximum damping) and the cam system has a radius $r_{cam} = 15mm$, the resulting total energy is

$$W_{tot} = W_\phi - (W_z + W_t) = -188.4mJ \qquad (16)$$

e.g. approximately 4.1 times more energy needs to be pumped in than can be gained (see also Figure 6) – considering no additional involved rotor dynamics for the z_R movement, eq. (11); for simulations with rotor dynamics, see [3]. Using existent low friction cam setups in examined study, when the damping coefficient is set accordingly low, an overall energy surplus might result. Therefore, using a nonresonant oscillator [1], [3] with a cam system, it is not unrealistic with a low friction cam setup to create an overall energy surplus. Note also, that infinite other stator-rotor PM configurations exist (the one discussed here could be stacked in z-direction) and it seems that the active patent [17] might describe one of such stator-rotor PM configurations.

In case a parametric resonant oscillator [1] is used, no cam at all is needed, as the lateral (quasi-periodic) movement is created elegantly with the rotor inertia and a radial and lateral PM spring system.

Conclusions

It is stated that, in theory, by combining trajectories of a rotor with accordingly stator-rotor PM distributions, an asymmetric incommensurable torque signal is feasible. The presented trajectories have been limited in rotational- (ϕ) and translational- (z) direction, excluding movements that involve also radial direction (changing rotor diameter distance r, see also Figure 1). However, we showed with three different approaches the same asymmetric incommensurable torque signal can be numerically simulated based on well accepted classic EM theory only. Also important in this study is the foresight, that magnet field distributions can exert energy and are not per se conservative fields. According to the presented results, the magnetic field itself is neither conservative nor non-conservative; it

all depends on the closed path trajectories followed through the field. Non-conservative trajectories can be generated which allow netto work while rotating a rotor over one full revolution – if the inevitable accompanied force signal (compare Figure 7) is accordingly damped in the cam-channel. The fundaments for the forecasted energy source, which is necessary to deliver this netto work, remain a research question, and further open-source experiments are indispensable to verify the presented theoretical claims.

References

[1] L. Kurmann and Y. Jia, "Oscillators with Nonpolar Magnetic Repulsion System and its Use in Rotary Nonresonant and Resonant Kinetic Energy Harvesters," *IOSR Journal of Applied Physics*, vol. 10, no. 4, pp. 57–76, 2018.

[2] J. L. Duarte, "Modeling the Yildiz Motor revisited," *Eindhoven University of Technology Research Report*, DOI: 10.6100/6B67487A-BD78-4A24-BDD1-D7B9B3DBD5B7, 2018.

[3] L. Kurmann and J. L. Duarte, "Generation of asymmetric incommensurable torque signals," *J. Phys.: Conf. Ser.*, vol. accepted, published in Dec. 2018, 2018.

[4] F. U. Khan, "Review of non-resonant vibration based energy harvesters for wireless sensor nodes," *Journal of Renewable and Sustainable Energy*, vol. 8, no. 4, p. 44702, 2016.

[5] A. Z. Trimble, J. H. Lang, J. Pabon, and A. Slocum, "A Device for Harvesting Energy From Rotational Vibrations," *J. Mech. Des.*, vol. 132, no. 9, p. 91001, 2010.

[6] E. M. Yeatman, "Energy harvesting from motion using rotating and gyroscopic proof masses," *Proceedings of the Institution of Mechanical Engineers, Part C: Journal of Mechanical Engineering Science*, vol. 222, no. 1, pp. 27–36, 2008.

[7] D. P. Arnold, "Review of Microscale Magnetic Power Generation," *IEEE Trans. Magn.*, vol. 43, no. 11, pp. 3940–3951, 2007.

[8] E. Arroyo and A. Badel, "Electromagnetic vibration energy harvesting device optimization by synchronous energy extraction," *Sensors and Actuators A: Physical*, vol. 171, no. 2, pp. 266–273, 2011.

[9] B. P. Mann and B. A. Owens, "Investigations of a nonlinear energy harvester with a bistable potential well," *Journal of Sound and Vibration*, vol. 329, no. 9, pp. 1215–1226, 2010.

[10] Y. Jia, J. Yan, K. Soga, and A. A. Seshia, "Parametric resonance for vibration energy harvesting with design techniques to passively reduce the initiation threshold amplitude," *Smart Mater. Struct.*, vol. 23, no. 6, p. 65011, 2014.

[11] M. Flankl, "Range Contactless Electromechanical Energy Harvester Facing a Moving Conductive Surface," (eng), http://ieeexplore.ieee.org/servlet/opac?punumber=7298093, 2015.

[12] D. Spreemann, Y. Manoli, B. Folkmer, and D. Mintenbeck, "Non-resonant vibration conversion," *J. Micromech. Microeng.*, vol. 16, no. 9, S169-S173, 2006.

[13] Y. Klevis, "Human Motion Energy Harvesting: Numerical Analysis of Electromagnetic Swing-Excited Structures,"

[14] S. P. Beeby *et al.*, "A micro electromagnetic generator for vibration energy harvesting," *J. Micromech. Microeng.*, vol. 17, no. 7, pp. 1257–1265, 2007.

[15] L. Kurmann *et al.*, "Autoparametric Resonance Systems for Vibration-Based Energy Harvesters," *J. Phys.: Conf. Ser.*, vol. 660, p. 12070, 2015.

[16] L. Kurmann, Y. Jia, Y. Manoli, and P. Woias, "Magnetically levitated autoparametric broadband vibration energy harvesting," *J. Phys.: Conf. Ser.*, vol. 773, p. 12006, 2016.

[17] M. Yildiz, "Device having an arrangement of magnets," WO 2009/019001 A3 2009/019001 A3.

[18] S. J. Chapman, *Electric machinery fundamentals*, 4th ed. New York NY: McGraw-Hill Higher Education, 2005.

[19] D. J. Griffiths, *Introduction to electrodynamics*, 3rd ed. Upper Saddler River, N.J.: Prentice Hall; London : Prentice-Hall International, 1999.

[20] L. Kurmann, "Rotary Nonresonant Energy Harvesting," IMTEK, Albert-Ludwigs-University Freiburg im Breisgau, 2018 (under review).

[21] S. Babic and C. Akyel, "Magnetic Force Between Inclined Circular Filaments Placed in Any Desired Position," *IEEE Trans. Magn.*, vol. 48, no. 1, pp. 69–80, 2012.

[22] S. I. Babic and C. Akyel, "Magnetic Force between Inclined Circular Loops (Lorentz Approach)," *PIER B*, vol. 38, pp. 333–349, 2012.

[23] D. Spreemann and Y. Manoli, *Electromagnetic Vibration Energy Harvesting Devices: Architectures, Design, Modeling and Optimization*. Dordrecht: Springer Netherlands, 2012.

[24] M. Charu, D. Warren, S. Wallace, and H. Guoqiang, *A New Continuously Differentiable Friction Model for Control Systems Design*. Piscataway N.J.: IEEE, 2005.